Validation of Vehicle Panel/Equipment Response From Diffuse Acoustic Field Excitation Using Spatially Correlated Transfer Function Approach.

Andrew Smith.[1]
NASA/Marshall Space Flight Center, Huntsville, AL 35612

Bruce LaVerde[2]
ERC Inc, ESTS Group, Huntsville, AL 35806

Clay Fulcher[3]
Jacobs Engineering, ESTS Group, Huntsville, AL 35806

Ron Hunt[4]
Triumph Aerospace, ESTS Group, Huntsville, AL 35806

An approach for predicting the vibration, strain, and force responses of a flight-like vehicle panel assembly to acoustic pressures is presented. Important validation for the approach is provided by comparison to ground test measurements in a reverberant chamber. The test article and the corresponding analytical model were assembled in several configurations to demonstrate the suitability of the approach for response predictions when the vehicle panel is integrated with equipment. Critical choices in the analysis necessary for convergence of the predicted and measured responses are illustrated through sensitivity studies. The methodology includes representation of spatial correlation of the pressure field over the panel surface. Therefore, it is possible to demonstrate the effects of hydrodynamic coincidence in the response. The sensitivity to pressure patch density clearly illustrates the onset of coincidence effects on the panel response predictions.

Nomenclature

Acronyms:

APTF	-	Acceleration/Pressure Transfer Function
ESTS	-	Engineering, Science, and Technical Services
FEM	-	Finite Element Model
MAC	-	Modal Assurance Criteria
MSFC	-	Marshall Space Flight Center
RMM	-	Response Matching Method

Modal Data:

$\Phi_j = \begin{bmatrix} \phi_{j1} & \phi_{j2} & \cdots & \phi_{jM} \end{bmatrix}$ - Mode shapes for bare skin at a few reference locations *j*,

$\omega = [\omega_1 \quad \omega_2 \quad \cdots \quad \omega_M]$ - Natural frequencies for modes 1 – *M* of bare skin,

[1] Vibroacoustics Specialist, MSFC/EV31, Marshall Space Flight Center, AIAA Member
[2] Vibroacoustics Lead Engineer, ERC Inc, 14901 Corporate Dr NW # E, Huntsville, AL, AIAA Member.
3 Structural Dynamics & Loads Specialist, Jacobs Engineering, 1500 Perimeter Parkway, Huntsville, AL, AIAA Member.
[4] Structural Dynamics Analyst, Triumph Aerospace, 1500 Perimeter Parkway, Huntsville, AL, AIAA Member.

$\tilde{\Phi}_{\ell} = \left[\tilde{\phi}_{\ell 1} \quad \tilde{\phi}_{\ell 2} \quad \cdots \quad \tilde{\phi}_{\ell \tilde{M}} \right]$ - Mode shapes for component-loaded skin at locations ℓ,

$\tilde{\Psi}_{q} = \left[\tilde{\psi}_{q1} \quad \tilde{\psi}_{q2} \quad \cdots \quad \tilde{\psi}_{q \tilde{M}} \right]$ - Modal forces for component-loaded skin at locations *q*,

$\tilde{\omega} = [\tilde{\omega}_1 \quad \tilde{\omega}_2 \quad \cdots \quad \tilde{\omega}_{\tilde{M}}]$ - Natural frequencies for modes $1 - \tilde{M}$ of component-loaded skin.

Static Data:

$F_b = [F_{b1} \quad F_{b2} \quad \cdots \quad F_{bN_b}]$, $b = 1, 2, \ldots N_p$ - Force distribution on GRIDs for unit pressure on patches *b*,

$R_{bc} = \sqrt{(x_b - x_c)^2 + (y_b - y_c)^2 + (z_b - z_c)^2}$ - Distance between CGs of patches *b* and *c*.

Pressure Data:

$P_{ref}(\omega)$ - Reference pressure autospectrum.

$W_{bb}(\omega)$ - Scaling functions for non-uniform pressure autospectra over the entire skin. Calculate these to coincide with the zone autospectra specified in the Vibroacoustic Loads Databook if available. That is, use the same W_{bb} on patches within specified launch vehicle zones. Set W_{bb} to unity if unknown.

I. Introduction

Hardware design on a new launch vehicle program is subject to performance requirements, cost and schedule constraints, and manufacturing constraints. The goal of design is to achieve low weight, healthy margins of safety and adequate performance, while satisfying the cost, schedule, and manufacturing constraints. Although the design must meet the performance requirements and satisfy these constraints, neither the validation test nor the analysis is so constrained. Traditionally, hardware design has relied heavily on development and qualification testing programs. Within these programs, uncertainty is always present due to issues such as unit to unit variability, complexity in boundary conditions and measurement error/bias. Often the test conditions do not fully represent the flight environment for practical reasons; this departure can result in overly conservative test specifications and less efficient designs.

Today, programs are becoming increasingly reliant on computational simulations that provide more information but substitute testing with modeling uncertainty. A promising trend is the migration of the emphasis in test programs from hardware development toward experimental validation of the physics underlying a computer simulation.

Predicting the structural vibration response to broadband excitation of a fluid/structural panel interface is a challenging aspect of the design problem. Added complexity arises when equipment is mounted to the vehicle panel. NASA has identified a need to standardize the approach for predicting broad-band response of mass-loaded panel assemblies. Standardization of any approach requires experimental validation in a controlled environment. The analysis methodology and experimental validation described in this paper are offered in the spirit of contributing toward that end.

So that the validation via acoustic ground testing can be appreciated, a description of the test articles and ground test setup is provided. A flight-like vehicle panel is described with various mounted equipment configurations for a range of mass-loaded panel assemblies. Validation of an approach that makes use of analytical models can be accomplished more readily if model fidelity is known to be adequate for the intended purpose. Modal surveys of the test hardware were performed for this purpose; data showing favorable modal correlation of the hardware and the finite element models (FEM) developed for this study is provided.

In addition to the validation of the methodology, evidence will be supplied though convergence studies to evaluate the frequency range of interest for component interface forces and panel strains, parameters important to the design engineer. The convergence characteristics of these design metrics will be compared to local acceleration, velocity and displacement responses near the component mounts to determine which of the latter provides the best indication of force and strain convergence.

Two related methodologies for predicting response using a finite element approach will be presented. Equations have been developed using modal coordinates and are provided for ease of use in frequency response analysis. The methodologies depend upon transfer functions developed from the frequency response to a spatially correlated unit pressure field acting across the panel surface. The phasing of the applied forces is dependent on wave numbers of traveling pressure waves at the fluid/structure interface.

Several critical choices are made in the analysis to produce a convergent solution. To illustrate analytical convergence of the response, several parameter sensitivity studies were performed. The methodology presented includes a representation of the spatial correlation of a diffuse pressure field in the acceleration/pressure transfer function. Therefore, the effects of hydrodynamic coincidence may be demonstrated in the acceleration response to any applied diffuse-field pressure. The sensitivity to pressure patch density has proved to be an excellent way to illustrate the onset of coincidence effects on the panel assembly responses.

II. Ground Test Articles, Setup Description, and Modal Characterization

The vehicle panel test article is a cylindrical segment that could be assembled with other similar panels to construct a complete cylinder. For the purposes of configuring the panel in the wall of a reverberant chamber, a smaller representative section of the total circumference was desired. The panel has a smooth outer surface with orthogrid rib-stiffened construction on the interior surface. The material type is an aluminum alloy. It is approximately 81 inches in height. The outer surface is described by a diameter of 216.5 inches. The arc length is approximately equivalent to one eighth of the full cylinder circumference, which is approximately 85 inches. The test setup and views of the bare vehicle panel configuration are provided in **Figure 1**.

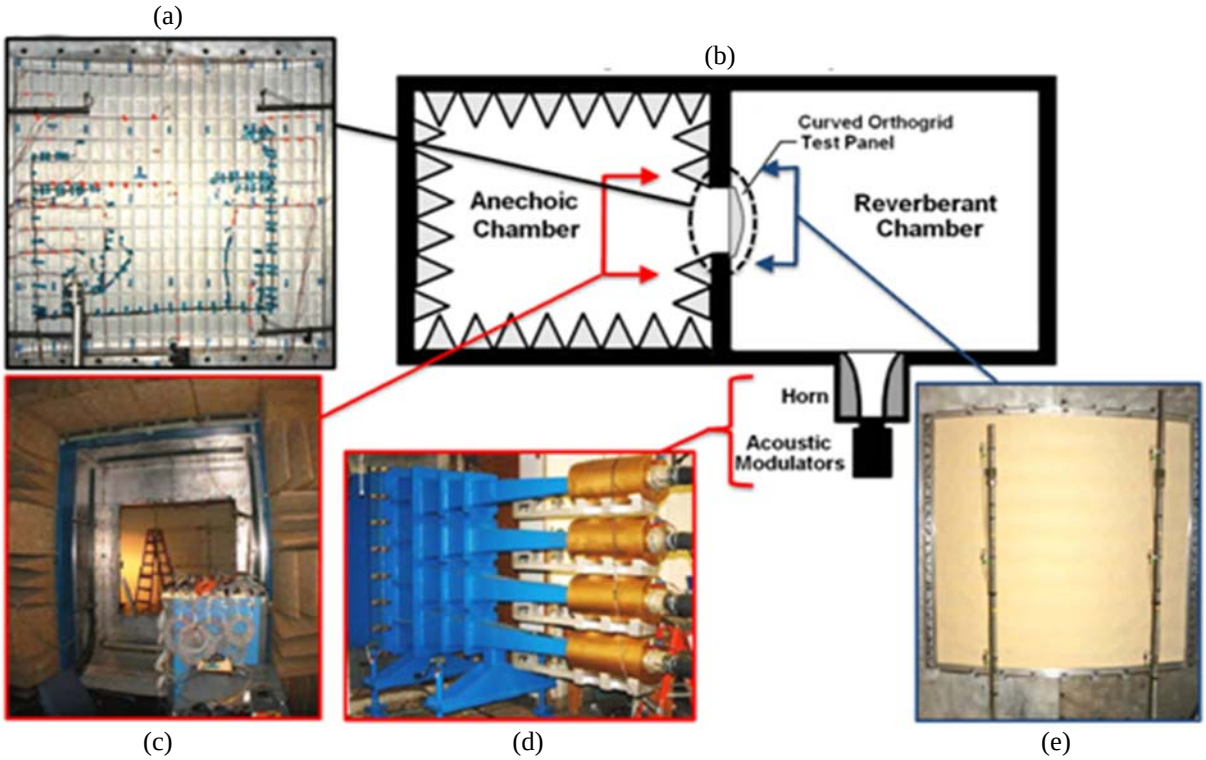

Figure 1. Ground acoustic test setup with vehicle panel test article mounted between two rooms. (a) Flight-Flight-like orthogrid vehicle panel, (b) Plan view of acoustic chamber next to anechoic with test article mounted in large window between rooms, (c) View from anechoic toward reverberant chamber prior to installation of vehicle panel, (d) flow modulators used with exponential horns to introduce sound energies into reverberant chamber, (e) convex curvature of vehicle panel facing reverberant chamber.

Also, several configurations of the test article for the test series included equipment mass simulators. One of these test configurations including an equipment mass simulator is depicted in **Figure 2**.

Figure 3 presents a comparison of modal characteristics of the FEMs used in the analysis to those of the "as-tested" hardware. The correlation study was completed using a dense array of response points in a series of Modal Survey Tests: 32 tri-axial accelerometers for the empty fixture, 77 tri-axial accelerometers for the bare panel, and 85 tri-axial accelerometers for each of the mass-loaded panel configurations. The mode frequency and shape correspondence using Modal Assurance Criteria (MAC), Cross-Orthogonality and qualitative mode shape depictions between the analytical and test results was observed to be excellent.

Figure 2. 1st example configuration of vehicle panel with large-mass simulator plus one increment plate.

Bare Panel Test and Analysis Correlation Summary

TEST MODE	TEST FREQ	FEM MODE	FEM FREQ	MAC	CROSS-ORTHOG	FREQ DIFF
1	101.21	1	97.20	0.96	-0.99	-4.0%
2	110.01	2	106.67	0.95	0.97	-3.0%
3	150.75	5	143.04	0.93	-0.91	-5.1%
4	159.82	7	155.33	0.94	-0.98	-2.8%
5	186.64	9	181.98	0.90	0.90	-2.5%
6	207.79	10	198.37	0.86	0.92	-4.5%
7	208.64	11	202.65	0.51	-0.54	-2.9%
8	218.95	14	211.19	0.92	0.98	-3.6%
9	242.66	17	233.96	0.75	-0.86	-3.6%
10	251.70	18	243.28	0.91	-0.97	-3.4%
11	281.13	21	268.45	0.39	0.60	-4.5%
12	291.97	26	283.18	0.75	-0.68	-3.0%
13	319.69	30	307.89	0.88	0.90	-3.7%

(a)

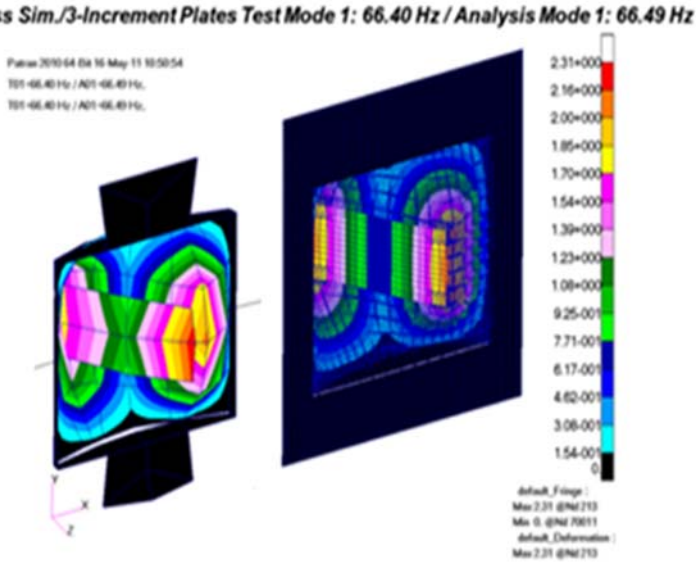

(b) MAC = 0.95 / Cross-Orthogonality = -0.96 / Frequency Difference = +0.1%

Figure 3. Example modal characteristic comparisons: (a) MAC and cross-orthogonality for the bare panel configuration, (b) Side-by-side mode shapes for one configuration of the test article with mass simulator.

III. Validation Comparison and Frequency Band of Interest

Validation of the method may be demonstrated by comparing the spectral densities of the measured and predicted responses at the transducer locations. Auto-spectral densities of the pressure field derived from microphone measurements were applied to the surface of the panel model. **Figure 4** shows several accelerometer locations on both the vehicle panel and the large equipment mass simulator. One confidence builder is that the methodology worked as well for the bare panel as it did for the equipment-loaded cases. The high degree of

correspondence is illustrated in overlays of measured and predicted accelerations in **Figure 5** and **Figure** 6. **Figure 5** compares accelerations at location 11 on the panel, and shows excellent agreement. Acceleration channels corresponding to three directions on the mass simulator at location 15 are compared in **Figure 6.** The measured and predicted responses are shown in blue and green respectively, with excellent agreement. If not for the appearance of noise floor from the measurement system which affects the axial response at location 15, the comparison would be even better. Again one of the most satisfying indicators that the methodology works is that the results compare well for different configurations of the model and hardware. In **Figure 8** both the bare panel and the large simulator plus 1 increment plate configurations are presented. The approach to determine the frequency band of interest for component interface forces

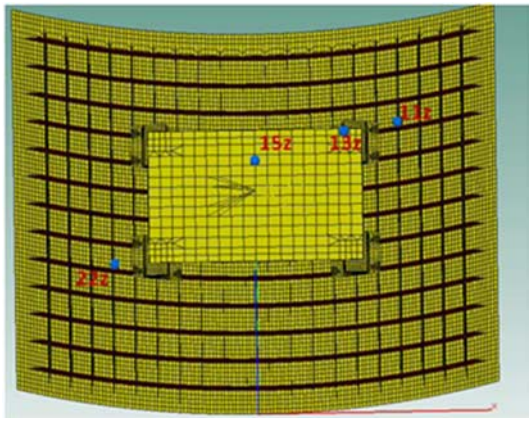

Figure 4. Example accelerometer locations used to demonstrate validation.

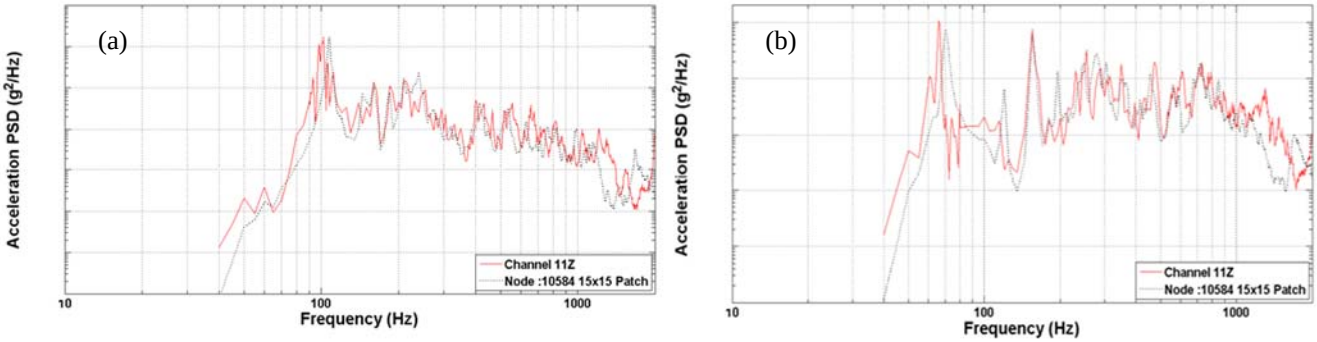

Figure 5. Validation response comparisons on vehicle panel test article at location 11z: (a) Bare panel response, (b) Response for vehicles panel with large simulator plus three increment plates

and panel strains was to plot the square root of the cumulative integral of the autospectral densities of each. The operation results in the accumulated root mean square (RMS) response over frequency. The cumulative RMS values of force and strain eventually flatten out at a certain frequency, as shown in **Figure 9** andFigure **10**. **Figure 9** provides one of the premier results of this report. In **Figure 9**, the cumulative RMS forces and strains are overlaid onto similar plots of cumulative RMS acceleration, velocity and displacement. This comparison is sufficient to show that force and strain converges more closely with velocity rather than displacement or acceleration. Therefore a consideration of the convergence of RMS velocity is a good indicator the upper frequency

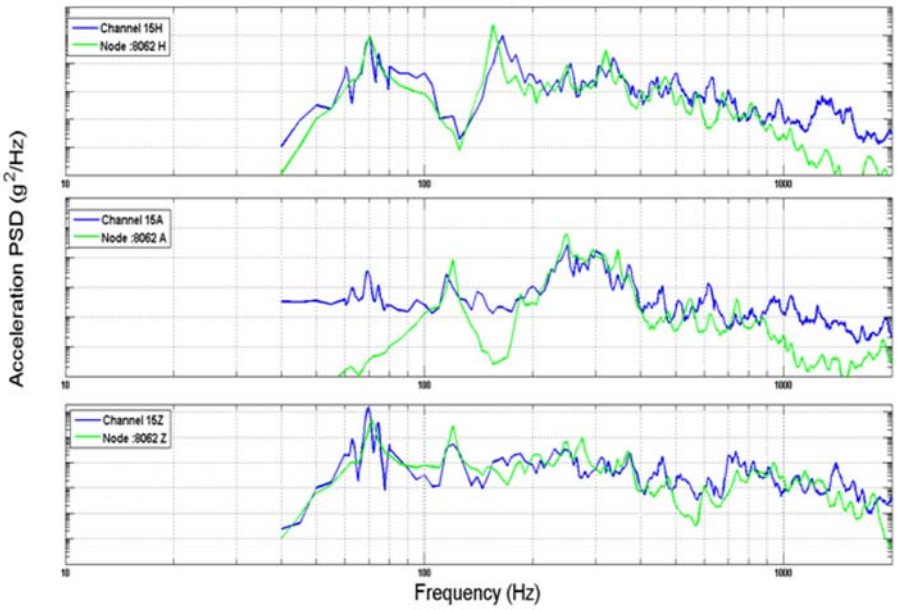

Figure 6. Acceleration at location 15 near center of large mass simulator plus one increment plate: (a) Hoop direction overlay, (b) Axial direction, (c) Z direction normal to plane of mass simulator.

limit needed for estimating component/panel interface force and panel stress and strain. **Figure 10** illustrates the reason that the velocity is such a good indicator for this frequency range. Examination shows that the high-frequency roll off of the velocity and strain spectral densities are similar. In this case ***a -12 dB/octave slope*** was plotted for comparison.

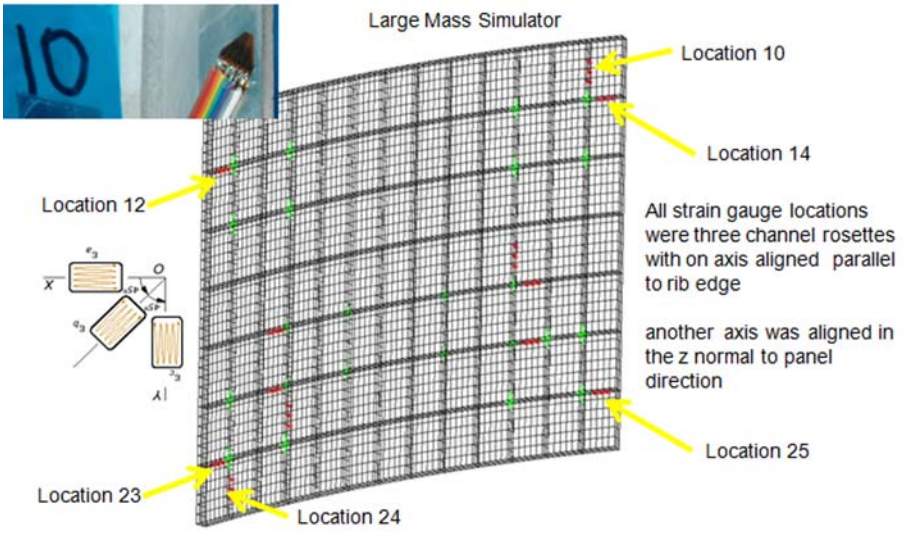

Figure 7. Array of strain gauge rosette locations appear marked in red. A close-up of location 10 on an axial rib appears in the upper left.

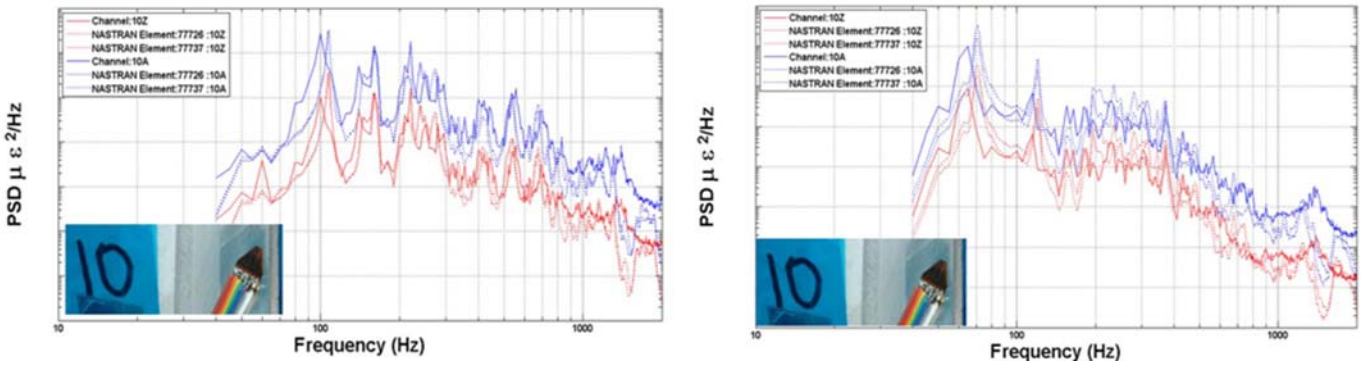

Figure 8. Validation response comparisons of strain on vehicle panel test article at location 10: (a) Bare panel response for two channels of the rosette. (b) Response for vehicle panel with large simulator plus 3 increment plates

IV. Methodology Presentation

Two related methodologies for calculating response using a finite element based approach are presented in this section. The equations provided have been fully developed using modal coordinates for ease of use in frequency response analysis. The methodologies are dependent upon development of transfer functions from the spatially correlated forces represented in the pressure field acting across the panel surface. The phasing of applied forces is dependent on wave numbers of traveling pressure waves in the fluid at the interface with the structural panel.

The first method is referred to as the Acceleration/Pressure Transfer Function (APTF) Method. The name implies the use of a spatially correlated pressure field across the vehicle panel. This method requires knowledge of the autospectral density of pressure over the panel surface, and the normal modes from the integrated mass-loaded panel FEM. The spatial correlation of pressure over the surface is derived from the autospectra and a diffuse-field function of the sound velocity and panel geometry.

The second approach is referred to as the Response Matching Method (RMM). This method replaces constant mass ratio in Barrett with frequency-dependent response modulation (both attenuation and amplification). The modulation may be expressed as a ratio of vehicle characteristics such as response/input transfer functions, dynamic (apparent) mass (force / acceleration), or dynamic stiffness (force / displacement). This method requires both the definition of measured or estimated bare panel accelerations at selected reference points, and also a pair of response/drive-point transfer functions describing the dynamic masses and the dynamic stiffness. These should be measured or derived from the following:

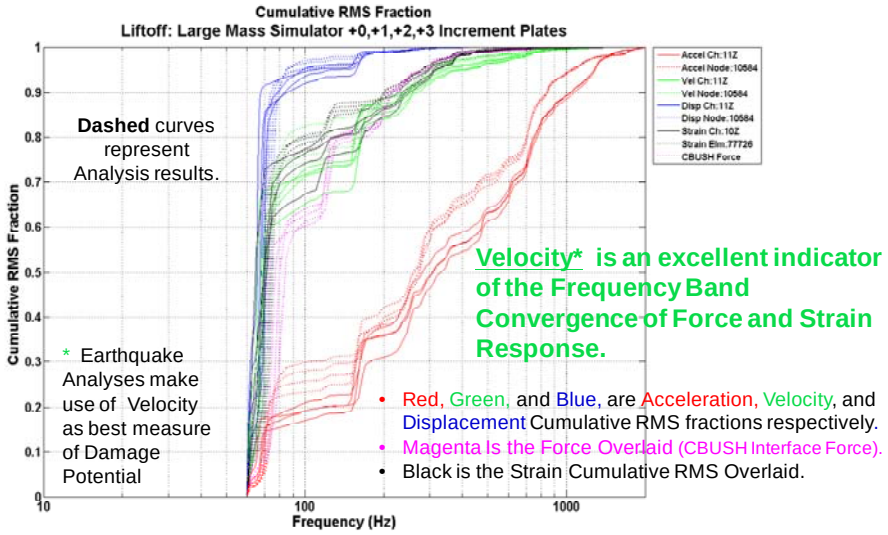

Figure 9. Illustrates from both measured and analytical results that velocity converges through 90-100% of cumulative RMS in about the same frequency band as the strain and the force.

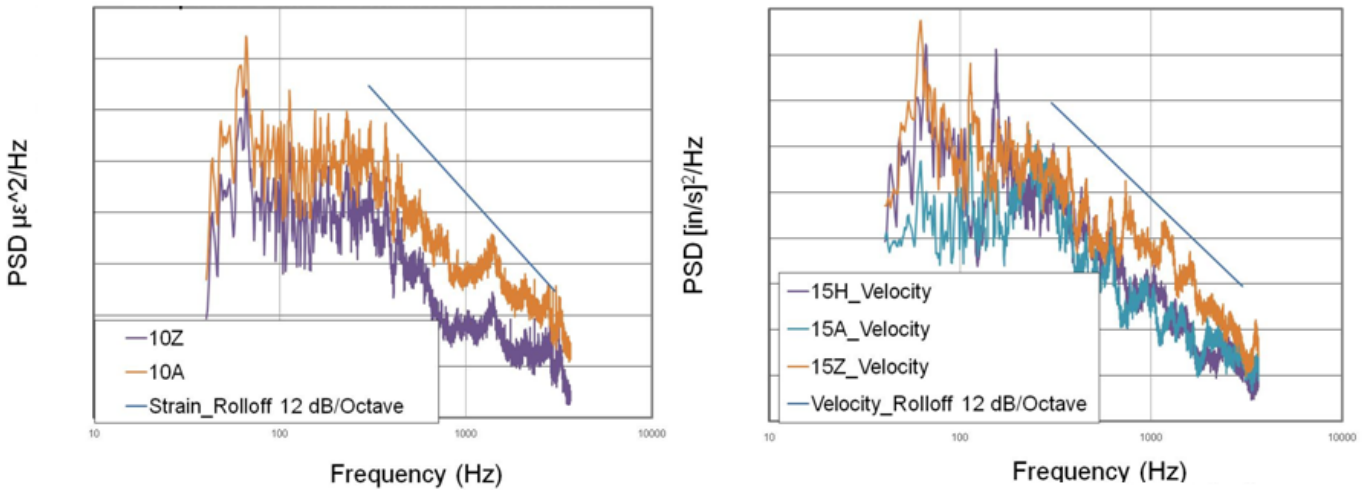

Figure 10. Illustrates similarity in roll-off at high frequency: (a) Spectral density for measured strain at location 10 near the equipment interface with the vehicle panel, (b) Spectral density for velocity at location 15 on the large mass simulator

1. Normal modes for the "integrated mass-loaded configuration" developed from test or FEM
2. Normal modes for the Bare Panel Configuration from test or FEM.
3. Estimate of vibration response spectral density for the bare panel configuration from measurement data bank or from APTF.

The APTF method has been realized in this paper by solving for the normal modes in MSC NASTRAN and importing the modal results into MATLAB to calculate response:

Definition of the correlated pressure forcing function is the average narrowband pressure PSD from a test case at a typical liftoff level which is assumed to be diffuse over the frequency range from 20-2000 Hz. (average of 6 mics)

The normal modes were developed from either the correlated truth FEM or a number of other FEMS developed for sensitivity studies also presented in the paper.

Although the methodology plots for RMM are fully presented in this extended abstract, the validation comparisons are yet to be added. This addition for the RMM approach will be added prior to submitting the final paper. An overview of the flow for the two model based approaches is presented beside the traditional empirical scaling approach in **Figure 11**.

The APTF method and RMM are a matched set of approaches. For instance, when the vibration spectral density input to the second method, RMM, is an estimate developed using the direct pressure APTF method then the resulting vibration response estimate produced for the "integrated/mass-loaded system" from either of these two

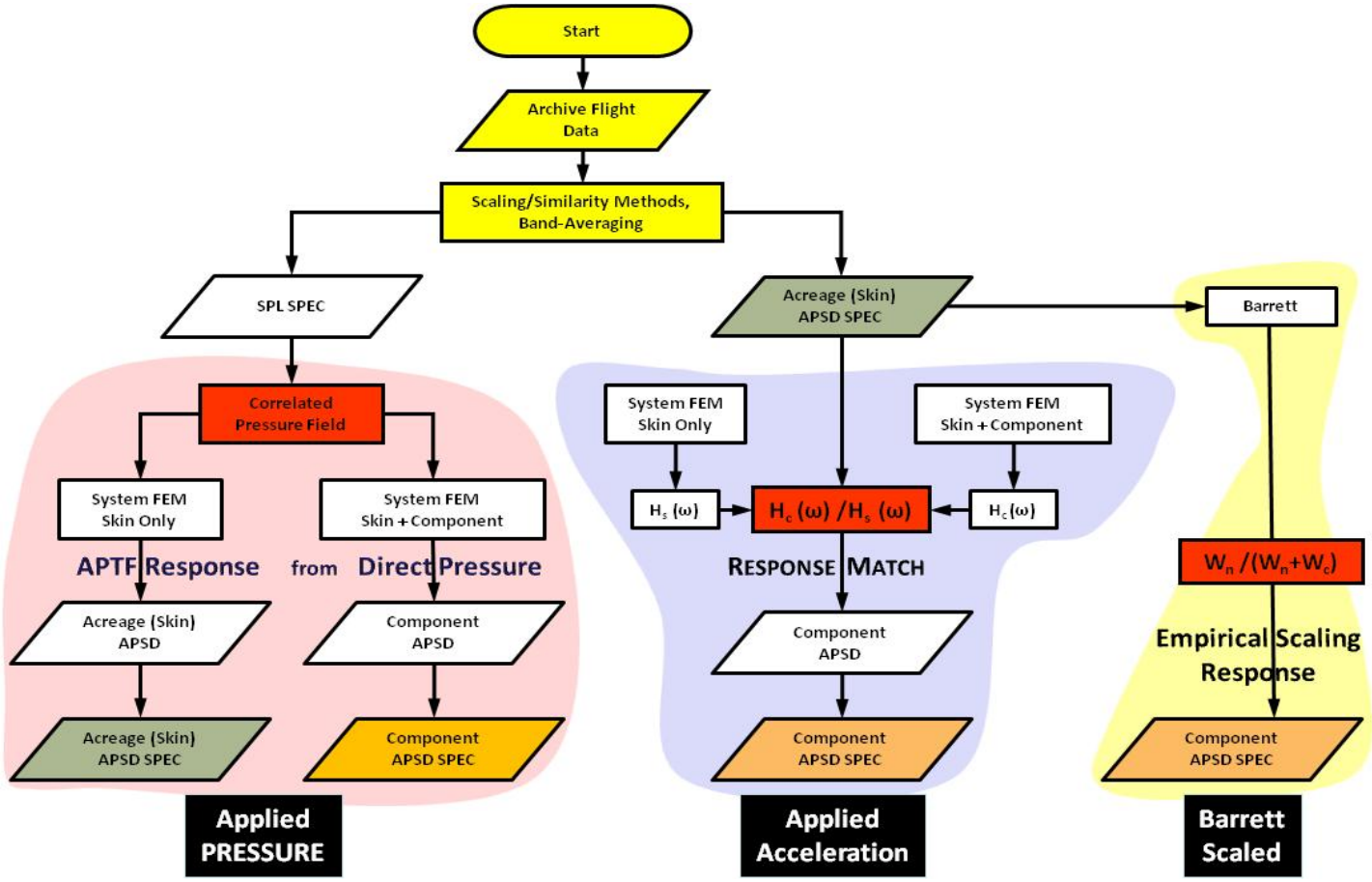

Figure 11. Methodology comparison flow diagram. Using databank of measurements as a starting point is an important practice useful to both semi-empirical and model based methods. When the vibration spectral density input to the second method, RMM, is an estimate developed using the direct pressure APTF method then the resulting vibration response estimate produced for the "integrated/mass-loaded system" from either of these two approaches will be identical.

approaches will be identical This is because the transfer functions on which they depend are also identical. But the APTF method is the preferred approach when the starting point is knowledge of the spatially correlated pressure field because solving for the bare panel response may then be unnecessary. The analyst is free to proceed directly to the integrated system response calculation in this case; direct pressure APTF estimation of integrated system response, only one set of normal modes is required:

1. Normal modes from evaluation of the integrated mass-loaded panel FEM
2. Definition of correlated pressure forcing function

So an important result that may be understood from the flow diagram and the equations that follow in this section is that as long as the correlated pressure forcing function is available as an input it is more efficient to proceed directly using the APTF method, however if the vibration response form a databank or test is more available

and perhaps more believable (for instance the acoustic measurements from a flight test were faulty due to some measurement system errors) then RMM can be a dependable alternative where the pressure definition is not needed.

The equations for the validated and very effective APTF and RMM approaches may be understood from the following equations and discussion. A random pressure field on a launch vehicle skin surface may be approximated by dividing the surface into "patches," or regions of uniform pressure with zero phase. The size of each patch must be chosen small enough to justify the assumption of uniform (though dynamically varying) pressure with zero phase across the patch.

The pressure may be defined as a stationary Gaussian random field with spatially varying autospectral density. The pressures on any pair of patches may be correlated, exhibiting a non-zero cross-spectral density between them. The random pressure field is thus a square Hermitian matrix of spectral densities of dimension N_p, the total number of pressure patches. The pressure autospectra occur on the diagonal of the matrix. The cross-spectra appear off of the diagonal. The random pressure field on all patches may be written as

$$\boldsymbol{\mathcal{P}}_{N_p}(\omega) = \begin{bmatrix} P_{11} & P_{12} & \cdots & P_{1N_p} \\ P_{21} & P_{22} & \cdots & P_{2N_p} \\ \vdots & \vdots & \ddots & \vdots \\ P_{N_p1} & P_{N_p2} & \cdots & P_{N_pN_p} \end{bmatrix} \tag{0}$$

where $P_{bc} = P_{cb}^*$, and the asterisk denotes the conjugate operator. If spatial functions $\gamma(\omega, R)$ are defined that relate the autospectra to the cross-spectra, (0) may be written as

$$\boldsymbol{\mathcal{P}}_{N_p}(\omega) = \begin{bmatrix} \gamma_{11}\hat{P}_{11} & \gamma_{12}\hat{P}_{12} & \cdots & \gamma_{1N_p}\hat{P}_{1N_p} \\ \gamma_{21}\hat{P}_{12} & \gamma_{22}\hat{P}_{22} & \cdots & \gamma_{2N_p}\hat{P}_{2N_p} \\ \vdots & \vdots & \ddots & \vdots \\ \gamma_{N_p1}\hat{P}_{1N_p} & \gamma_{N_p2}\hat{P}_{2N_p} & \cdots & \gamma_{N_pN_p}\hat{P}_{N_pN_p} \end{bmatrix} \tag{0}$$

where $\hat{P}_{bc} = \sqrt{P_{bb}P_{cc}}$ and γ_{bb} have been added to the diagonals for generalization. The expression for $\hat{P}_{bc}$ arises from an inequality requirement on the coherence which states that

$$0 \le \frac{\left|P_{bc}(\omega)\right|^2}{P_{bb}(\omega)P_{cc}(\omega)} \le 1.0 \tag{0}$$

For a diffuse field, the spatial functions γ may be expressed as

$$\gamma_{bc}(\omega, R_{bc}) = \frac{\sin\left(R_{bc}\,\kappa(\omega)\right)}{R_{bc}\,\kappa(\omega)} \tag{0}$$

where R_{bc} is the distance between the area CGs of patches *b* and *c*, $\kappa(\omega) = \omega / C_o$, and C_o is the speed of sound through the fluid medium adjacent to the patch material. The patch CGs are constrained to lie on the curved skin surfaces. When *b* = *c*, the spatial functions coincide with the patch autospectra, the distance R between patches vanishes and $\gamma_{bb} \rightarrow 1.0$ in the limit as $R_{bb} \rightarrow 0$ (L'Hopital's Rule). Finally, the patch autospectra may be expressed as products of frequency-dependent scaling functions $W_{bc}(\omega)$ and an arbitrary reference autospectrum. (e.g., one of the patch autospectra could be selected, but this is not required.)

$$P_{bb}(\omega) = W_{bb}(\omega) P_{ref}(\omega) \tag{0}$$

Substituting (0) into (0) we obtain an expression for the diffuse-field pressure model used for the lift-off environments in this study:

$$\boldsymbol{\mathcal{P}}_{N_p}(\omega) = \begin{bmatrix} \gamma_{11} W_{11} & \gamma_{12} W_{12} & \cdots & \gamma_{1N_p} W_{1N_p} \\ \gamma_{12} W_{12} & \gamma_{22} W_{22} & \cdots & \gamma_{2N_p} W_{2N_p} \\ \vdots & \vdots & \ddots & \vdots \\ \gamma_{1N_p} W_{1N_p} & \gamma_{2N_p} W_{2N_p} & \cdots & \gamma_{N_pN_p} W_{N_pN_p} \end{bmatrix} P_{ref} \tag{0}$$

where $W_{bc}(\omega) = \sqrt{W_{bb}(\omega)\, W_{cc}(\omega)}$. It is important to recognize that all of the pressure auto and cross-spectra represented in eqs (0) – (0) are known, and are related to the reference spectrum P_{ref} through the scaling functions. If the scaling functions are unknown, then the skin structure under consideration must be limited to regions with similar pressure autospectra and W_{bb} must be set to unity. The scaling functions may also be grouped into fewer distinct sets for large regions showing uniform pressure autospectra. That is, many of the functions may be assigned the same value for various zones of the launch vehicle even if the zone is subdivided into many patches.

Now consider the acceleration frequency response $a_u(\omega)$ at a point *j* on the skin to a unit oscillating pressure $p_u(\omega) = \cos(\omega t)$ on patch *b*. The frequency response is also the transfer function between any acceleration response $a_j(\omega)$ at *j* to arbitrary pressure $p_b(\omega)$ on patch *b*. Note that the response point locations are unrestricted. They may be located either within or external to the patch. In NASTRAN, the unit pressure is distributed as a set of non-uniform forces on the GRIDs comprising the shell elements within the patch. This non-uniform force distribution for a unit pressure may be obtained with an OLOAD request at the patch GRIDs in NASTRAN SOL 101. The force distribution may then be swept through the frequency range of interest to obtain the frequency response. The acceleration/pressure transfer function for a single patch may be expressed explicitly as the sum of weighted acceleration/force transfer functions. The weighting factor is the static force F_k at each input location *k* on the patch due to a unit pressure (from an OLOAD request in SOL 101):

$$H_{a_j/p_b}(\omega) = \sum_{k=1}^{N_b} \left\{ F_k \cdot \sum_{m=1}^{M} \left[\frac{-\omega^2 \phi_{jm} \phi_{km}}{\omega_m^2 - \omega^2 + i\, 2 \zeta_m \omega_m \omega} \right] \right\} \tag{0}$$

where

$H_{a_j/p_b}(\omega)$ is the transfer function between acceleration at point *j* and pressure p_b on patch *b*,

F_k is the static force at point *k* associated with a unit pressure on patch *b*,

ϕ_{jm} is the m^{th} mass-normalized mode shape at response point *j*,

ϕ_{km} is the m^{th} mass-normalized mode shape at point *k* in the pressure patch,

ω is the circular frequency,

ω_m is the circular natural frequency of mode *m*,

ζ_m is the critical damping ratio for mode *m*,

N_b is the number of GRIDs in the pressure patch,

M is the number of retained modes.

The acceleration PSD response $A_{jb}(\omega)$ to a random pressure $P_{bb}(\omega)$ on patch *b* is the squared magnitude of the acceleration/pressure transfer function in (0) multiplied by the pressure PSD, or

$$\begin{aligned} A_{jb}(\omega) &= \left|H_{a_j/p_b}(\omega)\right|^2 P_{bb}(\omega) \\ &= \left|H_{a_j/p_b}(\omega)\right|^2 W_{bb}(\omega) P_{ref} \end{aligned} \tag{0}$$

The total response at location *j* includes the autospectra from the pressures on all of the patches and also from non-zero cross-spectra between any two patches, or

$$\begin{aligned} A_j(\omega) &= \sum_b^{N_p} \left|H_{a_j/p_b}\right|^2 P_{bb} + \sum_b^{N_p}\sum_{c\neq b}^{N_p} H_{a_j/p_b} H^*_{a_j/p_c} P_{bc} \\ &= \sum_b^{N_p}\sum_c^{N_p} H_{a_j/p_b} H^*_{a_j/p_c} P_{bc} \end{aligned} \tag{0}$$

Expressing eq (0) in terms of the reference spectrum and the spatially dependent cross-spectra of eqs (0) and (0), we obtain

$$A_j(\omega) = \sum_b^{N_p}\sum_c^{N_p} \gamma_{bc} W_{bc} H_{a_j/p_b} H^*_{a_j/p_c} P_{ref} = \sum_b^{N_p}\sum_c^{N_p} \frac{\sin(\kappa R_{bc})}{\kappa R_{bc}} \sqrt{W_{bb} W_{cc}}\, H_{a_j/p_b} H^*_{a_j/p_c} P_{ref} \tag{0}$$

Note that the spatial functions γ reduce to unity for $b = c$, as mentioned previously. Eq (0) may be expressed in matrix form for computational efficiency in Matlab as

$$A_j(\omega) = \left[\mathrm{H}_{a_j} \sqrt{\mathrm{W}}\ \Gamma \sqrt{\mathrm{W}}\ \mathrm{H}^{\dagger}_{a_j} \right] P_{ref} \tag{0}$$

where † denotes the Hermitian conjugate and

$$\mathrm{H}_{a_j}(\omega) = \left[H_{a_j/p_1} \quad H_{a_j/p_2} \quad \cdots \quad H_{a_j/p_{N_p}} \right]$$ (a/p transfer functions from eq (0)),

$$\mathrm{W}(\omega) = \begin{bmatrix} W_{11} & & & 0 \\ & W_{22} & & \\ & & \ddots & \\ 0 & & & W_{N_p N_p} \end{bmatrix}$$ (pressure autospectra scaling functions from eq (0)),

$$\Gamma(\omega) = \begin{bmatrix} 1 & \frac{\sin(\kappa R_{12})}{\kappa R_{12}} & \cdots & \frac{\sin(\kappa R_{1N_p})}{\kappa R_{1N_p}} \\ & 1 & \cdots & \frac{\sin(\kappa R_{2N_p})}{\kappa R_{2N_p}} \\ & \mathrm{SYM} & \ddots & \vdots \\ & & & 1 \end{bmatrix}$$ (spatial functions from eq (0)).

If the pressure autospectrum does not vary significantly over the region of interest, $W_{bb}(\omega) = W_{cc}(\omega) \cong 1.0$, and eq (0) simplifies to

$$A_j(\omega) = \left[\mathrm{H}_{a_j} \, \Gamma \, \mathrm{H}_{a_j}^{\dagger} \right] P_{ref} \tag{0}$$

The term inside the bracket in eq (0) (or eq (0) for uniform pressure spectra) may be considered the squared transfer function between the total response at location j and the entire diffuse pressure field:

$$\left| H_{a_j/p}(\omega) \right|^2 = \mathrm{H}_{a_j} \sqrt{\mathrm{W}} \; \Gamma \sqrt{\mathrm{W}} \; \mathrm{H}_{a_j}^{\dagger} = \frac{A_j(\omega)}{P_{ref}(\omega)} \tag{0}$$

Note that $H_{a_j/p}$ is not an unchanging characteristic of the system since the scaling functions W depend upon the generally non-uniform patch autospectra which change at different points in the launch trajectory. However, if the random pressure may be considered uniform over the surface of interest, $H_{a_j/p}$ is characteristic of the system independent of input pressure or the output acceleration.

Eq (0) may be used to calculate $A_j(\omega)$ if the reference pressure P_{ref} and scaling functions W are known. Conversely, an effective reference pressure $\overline{P}_{ref}(\omega)$ may be calculated if the acceleration PSD is specified and W is set to the identity matrix. The locations *j* selected as reference points on a skin without mounted components should be few, and chosen as far as possible from zone boundaries, joints, or local skin features such as cutouts, or doublers.

Now consider the case when a component is mounted to the skin. The applied pressure does not change, but the transfer function in (0) developed for the bare skin must be generated for the component-loaded skin. Eqs (0) – (0) are applied at a response location ℓ using the modes of the component-loaded skin, and (0) becomes

$$\left| \tilde{H}_{a_\ell/p}(\omega) \right|^2 = \tilde{\mathrm{H}}_{a_\ell} \sqrt{\mathrm{W}} \; \Gamma \sqrt{\mathrm{W}} \; \tilde{\mathrm{H}}_{a_\ell}^{\dagger} = \frac{\tilde{A}_\ell(\omega)}{P_{ref}(\omega)} \tag{0}$$

where the tilde denotes the component-loaded acceleration/pressure transfer function and skin response. If the pressure is unknown, but the acceleration on the unloaded skin is known from measured flight data, the component-loaded response at any point ℓ may be obtained by eliminating $P_{ref}(\omega)$ from (0) and (0):

$$\tilde{A}_\ell(\omega) = A_j(\omega) \cdot \frac{\left| \tilde{H}_{a_\ell/p}(\omega) \right|^2}{\left| H_{a_j/p}(\omega) \right|^2} \tag{0}$$

where the acceleration/single-patch pressure transfer functions $H_{a_j/p_b}(\omega)$ in eq (0) for the bare skin are obtained from eq (0), and $\tilde{H}_{a_\ell/p_b}(\omega)$ in eq (0) for the component-loaded skin from

$$\tilde{H}_{a_\ell/p_b}(\omega) = \sum_{k=1}^{N_b} \left\{ F_k \cdot \sum_{m=1}^{\tilde{M}} \left[\frac{-\omega^2 \, \tilde{\phi}_{\ell m} \, \tilde{\phi}_{k m}}{\tilde{\omega}_m^2 - \omega^2 + i \, 2 \, \tilde{\zeta}_m \, \tilde{\omega}_m \, \omega} \right] \right\} \tag{0}$$

Equation (0) defines the Response Matching Methodology (RMM) for predicting the response of a component-loaded skin structure when the bare skin response is known, and the acceleration/pressure transfer functions for both bare and component-loaded skins are available from modal analysis of the respective skin models, or from modal testing. The frequency-dependent ratio of transfer functions in (0) replaces the Barrett scaling factor given by

$$B = \frac{w_n}{w_n + w_c} \tag{0}$$

where w_n and w_c are the weights of the bare and component-loaded structures, respectively.

Force and moment responses at specified interface elements (e.g., CBUSH) may be obtained in the same fashion by replacing the first mode shape term in (0) with the modal forces and moments obtained in a NASTRAN RESTART in SOL 103. The $-\omega^2$ term in the numerator of eq (0) is also dropped. The expression for the response force (or moment) at location *q* is similar to that for acceleration in (0):

$$\tilde{F}_q(\omega) = A_j(\omega) \cdot \frac{\left|\tilde{H}_{f_q/p}(\omega)\right|^2}{\left|H_{a_j/p}(\omega)\right|^2} \tag{0}$$

where $\tilde{F}_q(\omega)$ is the force (or moment) PSD at location *q*, and $\tilde{H}_{f_q/p}$ is the transfer function between the total force (or moment) at location *q* and the pressure:

$$\left|\tilde{H}_{f_q/p}(\omega)\right|^2 = \tilde{\mathrm{H}}_{f_q} \sqrt{\mathrm{W}}\ \Gamma \sqrt{\mathrm{W}}\ \tilde{\mathrm{H}}^{\dagger}_{f_q} = \frac{\tilde{F}_q(\omega)}{P_{ref}(\omega)} \tag{0}$$

The individual transfer functions $\tilde{H}_{f_q/p_b}(\omega)$ in $\tilde{\mathrm{H}}_{f_q}$ between the force at location *q* and each single-patch pressure on any patch *b* are given by

$$\tilde{H}_{f_q/p_b}(\omega) = \sum_{k=1}^{N_b} \left\{ F_k \cdot \sum_{m=1}^{\tilde{M}} \left[\frac{\tilde{\psi}_{qm}\, \tilde{\phi}_{km}}{\tilde{\omega}_m^2 - \omega^2 + i\, 2\, \tilde{\zeta}_m\, \tilde{\omega}_m\, \omega} \right] \right\} \tag{0}$$

where $\tilde{\psi}_{qm}$ is the m^{th} modal force at location *q*.

V. Models and Analysis Choice Sensitivities

In order to demonstrate and validate the approach a series of high fidelity Finite Element Models were developed and later evaluated against modal survey test measured modal characteristics as described in section II provided at conference in a previous paper[5]. The test validated models were comprised completely of shell elements which explicitly represented the vehicle panel outer skin as well as the ribs comprising a regular orthogrid pattern. These did serve as the back bone of the validation analysis. The test verified models also included representations of the equipment mass simulators.

One of the parameters that were varied during the sensitivity studies was model form of the vehicle panel. This required the development of a series of additional models. One set was comprised of smeared properties developed using the technique most often employed to represent rib stiffened vehicle panels as a layered composite. This technique permits the most flexibility to coarsen a panel mesh since the location of rib stiffeners need not be represented explicitly by the model nodes. Another modeling technique that was explored was to replace the shell elements that explicitly represented the ribs with beams. Several different mesh densities were also used in trials for each of the three modeling techniques.

Perhaps the most interesting sensitivity study addressed the choice of patch density for the frequency response analysis. Choosing an adequate patch density over which to apply the spatially correlated pressure field turned out to be critical for producing an estimate that converges to the measured solution. The array of modeling choices and patch densities that were considered is summarized in **Figure 12**. Some examples of patch density arrangements are presented in **Figure 13**.

[5] Maasha, R. et al.

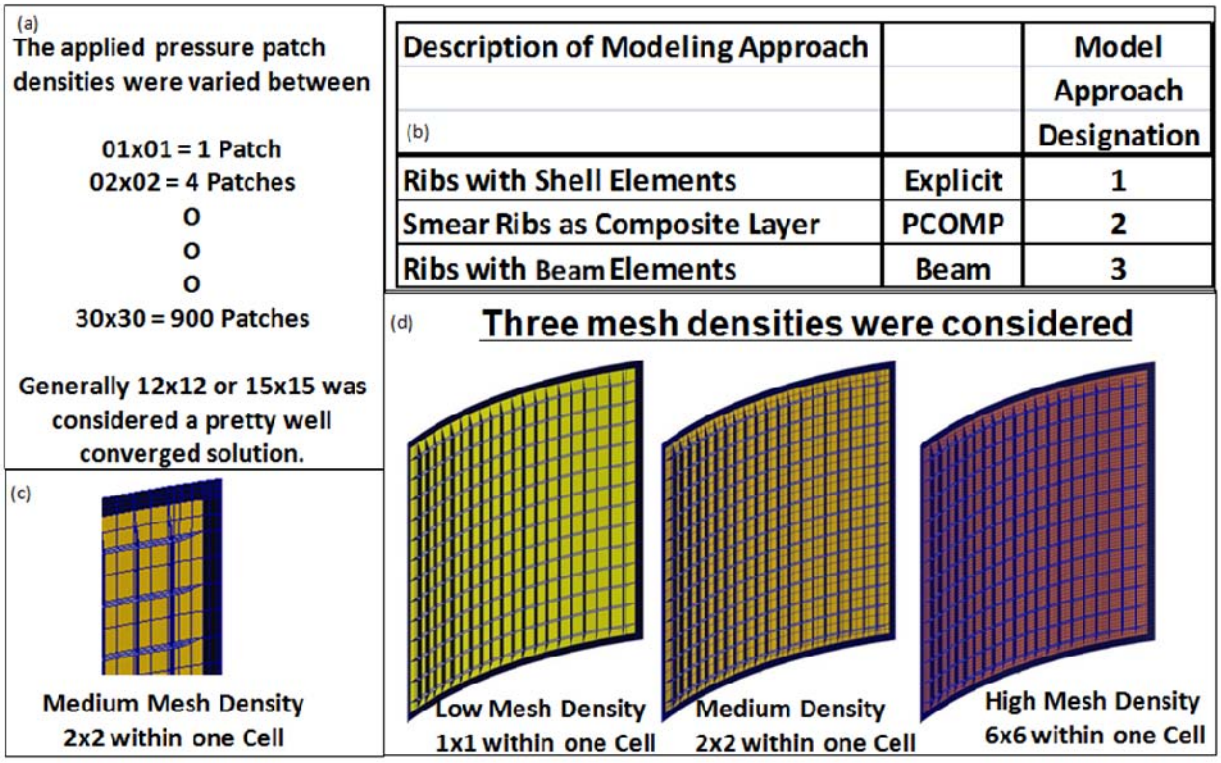

Figure 12. Summary of model and patch density sensitivity choices: (a) patch density sensitivity, (b) model form, (c) mesh density example, (d) mesh densities considered.

Figure 14 illustrates that the wrong choice of patch density can result in poor estimates of the vibration response. Choosing a patch density that is too coarse is likely to produce an under estimate of vibration response at higher frequencies at or above the hydrodynamic coincidence frequency. Coincidence is estimated to be very near 400 Hz for the bare vehicle panel tested. There is also the possibility that certain special cases of a coarse inadequate Patch density can produce overestimates of low frequency peaks. Under these unlucky circumstances an analyst might fool himself into an overestimate of interface load. The following explanation is offered for why these inadequate patch density choices may lead to erroneous results:

Figure 13. Patch density examples.

1. If you use an adequate patch density you will increase the fidelity of your high frequency response estimate. Convergence of the solution can be seen from below as patch density increases for the high frequency results. This is because the phasing of forces on surface nodes induced by the pressure field should change from positive and negative in certain regions based on the wave length of sound in the fluid and the angel of incidence on the panel. But the wavelengths are different at each frequency. As Frequency increases the wavelength decreases and you need a smaller, denser array of patches to get the correct answer. This is especially true at and above the coincidence frequency where the waves are said to be acoustically fast.
2. We also observed that certain cases of an inadequate patch density could over predict the Low frequency response. This is because the wavelengths of high frequency energy are represented incorrectly in too coarse a manner. The cases that over predicted happened to be patch arrangements that accidentally lined up with structural response flexural mode shapes. So we showed that it was possible to fool yourself if the patch density was too coarse and coincidentally was effective at exciting one or several important low frequency resonant modes. Figure 14 is the best illustration of this point. The bar chart indicates that one of our coarse patch density cases (2x2) over predicted the overall RMS. Examining the cumulative RMS curves shows a trace that is significantly higher than the converged solution just above 100 Hz. And the acceleration PSD overlays depict some overshoot traces on the 1st, 3rd, and 4th peaks. So over prediction of load is possible but the circumstances require a special alignment of patches with structural modes.

The upshot is that making sure you have an adequate patch density will protect you from both errors. Selecting a patch density so that the patch dimensions (or distance from one patch cg to the next) are ¼ of the wavelength of your highest frequency of interest is a rule of thumb that can provide adequate results.

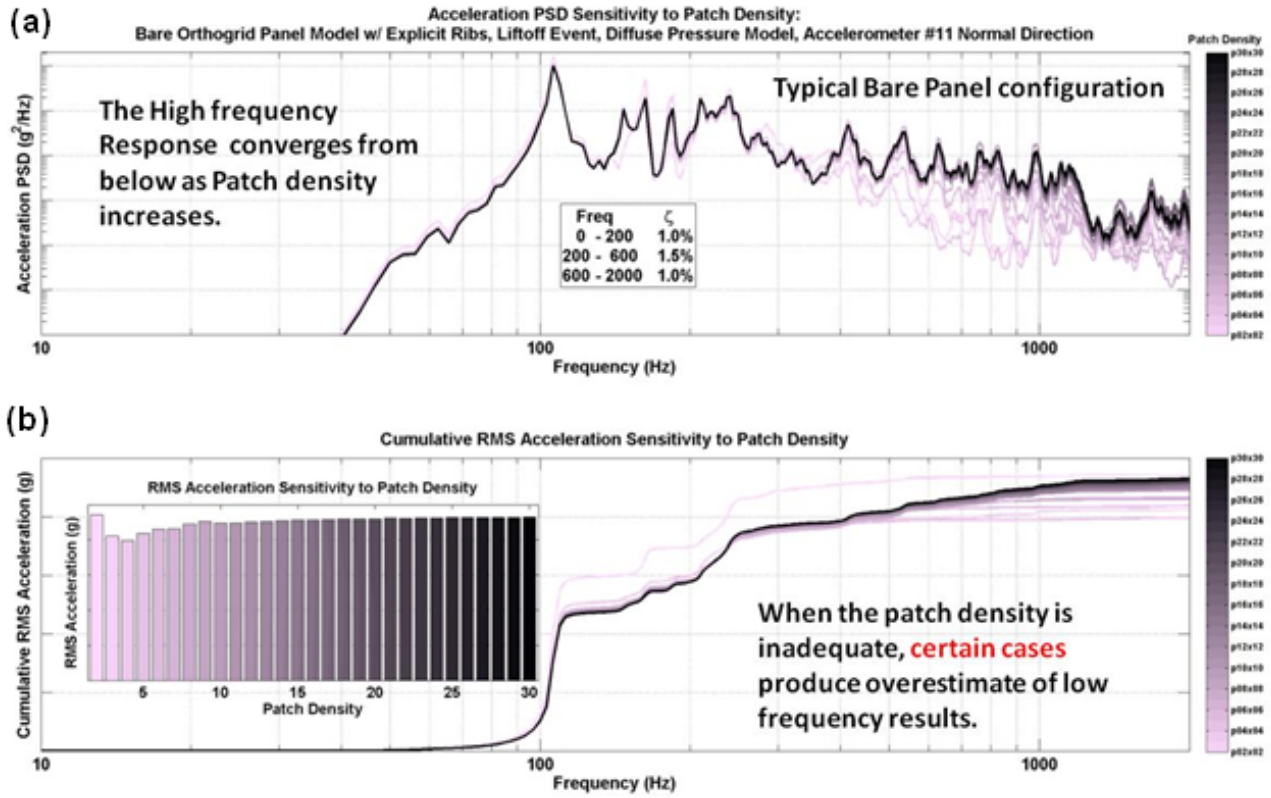

Figure 14. Example of patch density sensitivity comparisons: (a) The acceleration spectral density overlays from patch density sensitivity analysis cases show that at and above the coincidence frequency the solution converges from below with increasing patch density, (b) The cumulative RMS overlays indicate that certain cases of coarse patch densities have the drawback of over-predicting low frequency response.

VI. Conclusions

The current climate of tighter budgets will most likely demand more efficient processes for component design and for the development of component environments. Increased efficiency may be realized with test-validated system-level modeling and simulation. We recommend a refocusing of test program objectives. These objectives should migrate from hardware development toward experimental validation of computational models.

The acoustic testing of a flight-like vehicle panel with an array of equipment mass simulators provided a unique opportunity to introduce and validate these two methodologies (APTF & RMM). These methods deliver the capability to integrate and solve design issues on all sides of the interface (for instance propulsion and avionics components must integrate with the vehicle. All three organizations need design requirements).

Providing more optimum hardware designs – faster, lower cost, higher performance - should prove to be another advantage attained by the test validation of these additional methods already accomplished. The enhanced traditional methods which were semi-empirical sharpen the team to accomplish more. Empirical methods were linked to a class of design problems similar to the previous designs from which scaled results were pursued. The versatility of the newer methods is not infinitely robust, but has been shown to produce adequate estimates for a wide range of different configurations. Future tests may demonstrate some limitations as they also suggest the extent that we can broadens the range of design options using this type of analysis.

Modeling parameters have been identified and provided in this paper to serve as guidelines. The importance of these rules of was illustrated through sensitivity studies of patch and mesh densities, model form, and component weight.

Methodology to evaluate the frequency band of convergence (cutoff frequency) using a cumulative RMS calculation has also been presented. The lesson learned that the frequency range of interest for interface loads and strains correlate well with velocity provides a rationale to support use of a lower cutoff frequency than customary for some interface loads calculations. This has the potential to produce lower estimates of loads. For example, some early design loads have been calculated by using 3 times RMS in the frequency band out to 2000 Hz. A cut off frequency at 300-400 Hz would reduce these. The frequency range appropriate for cutoff can be evaluated for a particular design from estimates of velocity PSDs. The velocity spectral densities are used to determine convergence of the cumulative RMS. Note that this should not be done without using an adequate patch density.

Acknowledgments

The authors wish to thank both the MSFC ET40 Acoustic Test Lab and the Modal Test Lab for providing test results sufficient to validate both the Finite Element Models and the calculated response estimates using APTF and RMM.

References

1. Maasha, R., Towner, R., LaVerde B., Band, J., “Preliminary Correlation Results Summary for Mass-loaded Vehicle Panel Test Article Finite Element Models and Modal Survey Tests,” Proceedings of 2011 Spacecraft and Launch Vehicle Dynamic Environments Workshop, June 2011.
2. MSC.Software Corporation, MSC.ProCOR 2006 User’s Guide, 2006.
3. MSC.Software Corporation, MSC.NASTRAN 2008 User’s Guide, 2008.
4. MSC.Software Corporation, MSC.PATRAN 2010 User’s Guide, 2010.
5. MathWorks Inc., MATLAB Users Guide, 2010.
6. Craig, Roy, Structural Dynamics, An Introduction to Computer Methods, 1st ed., John Wiley & Sons, NY, 1981.
7. Chung, Y.T., “FEM Validation of Response Matching Method Final Report,” HDC-ARRA-8C-026, The Boeing Company, February 24, 2011.
8. Bendat, Julius and Piersol, Allan, Random Data Analysis and Measurement Procedures, 2nd ed., John Wiley & Sons, NY, 1986.
9. Peck, Smith, Fulcher, LaVerde & Hunt, "Development of Component Interface Loads on a Cylindrical Orthogrid Vehicle Section from Test-Correlated Models of a Curved Panel," Slide presentation at the Spacecraft & Launch Vehicle Dynamic Environments 2011 Workshop, The Aerospace Corp., El Segundo, CA, June 7-9, 2011.